JOURNAL OF MATERIALS SCIENCE 20 (1985) 3515–3523

The structure of a migrating low-angle tilt grain boundary in strontium titanate

M. FUJIMOTO*
Department of Materials Science and Engineering, Massachusetts Institute of Technology, Cambridge, Massachusetts 02139, USA

Weak beam transmission electron microscopy and stereomicroscopy have been used to characterize the three-dimensional structure of a severely deformed low-angle tilt grain boundary in a strontium titanate ceramic. Various interactions between crystal lattice dislocations and grain boundary dislocations in this boundary have been analysed. The deformed low-angle tilt grain boundary is a result of "partial glide". The boundary is composed of dislocations with Burgers vectors $a[\bar{1}00]$ and the deformation of the boundary is interpreted as having occurred by the interactions of the boundary with crystal lattice dislocations during grain boundary migration. Observed dislocation networks in the grain boundary are a result of the reaction $\mathbf{b}_3 = \mathbf{b}_1 + \mathbf{b}_2 = a[\bar{1}00] + a[00\bar{1}] = a[\bar{1}0\bar{1}]$, and the resultant dislocations are sessile. Also, many crystal lattice dislocations are pinned by the grain boundary and produce a complex dislocation structure for the boundary.

1. Introduction

In general, it is accepted that grain boundaries may migrate with a wide range of velocities which depend upon the magnitude of the driving force, the temperature, the composition, the external stress, and the grain boundary crystallography. Grain boundary migration is strongly related to grain boundary sliding, crystal growth, primary recrystallization and secondary crystallization. Therefore, there have been many experimental and theoretical studies of these phenomena. Some general reviews have also been reported on this topic in the last decade [1–7].

Studies of the relationship between grain boundary atomic structure and grain boundary migration have been performed in metals and NaCl [7–10]. Depending upon the structure of the grain boundary, a high-angle grain boundary can migrate due to its DSC lattice structure and its Burgers vector, but it has very rarely been reported to migrate under stress. On the other hand, a low-angle grain boundary can migrate, but most observations have reported extensive boundary sliding.

In these cases, the glide–climb movement and the appropriate shuffles lead to migration of the boundary. A crucial point is that each thermally activated diffusional jump can permit additional atoms to be transferred to the growing grain by shear processes or by shuffles according to the geometry of the boundary. The number of atoms transferred per diffusive jump depends upon the coincidence geometry of the boundary plane and the inclination of the Burgers vector of the grain boundary dislocation to the boundary plane.

Drastic deformation of migrating grain boundaries is frequently observed, which is a result of interactions between grain boundary dislocations and crystal lattice dislocations, segregated and/or precipitated impurities, and pores [11, 12]. In particular, break-away of the grain boundary depends upon its associated impurity cloud, and results from the growth of unstable velocity perturbations [7], and also escape of gliding crystal dislocation from their Cottrel atmospheres [9].

At the present time, manufacturers of perovskite-based dielectrics are facing reliability problems

*M. Fujimoto is a Visiting Scientist at the Massachusetts Institute of Technology on leave from Taiyo Yuden Co., Ltd., Tokyo, Japan.

0022–2461/85 $03.00 + .12

which are related to dislocations and oxygen diffusion. However, the characterization of dislocations and deformation mechanisms in perovskite materials has not been accomplished. In the observation of donor-doped strontium titanate ceramics by transmission electron microscopy (TEM) a low-angle tilt grain boundary deformed by interaction with crystal lattice dislocations was found. This particular grain boundary is shaped like a horseshoe. This configuration is unusual in deformed low-angle tilt grain boundaries, and has not been reported before. Strontium titanate is an ideal cubic perovskite material at room temperature and, therefore, an ideal material for observing dislocation processes.

It is the purpose of this paper to characterize the deformed structure in detail and discuss the implication of the observation on boundary mobility.

2. Experimental procedure

A mixture of equal amounts of $SrCO_3$ and TiO_2 with Nb_2O_5 (0.002 mol%) of chemical reagent grade (> 99% purity) was mixed by wet milling for 20 h. The mixture was calcined at 1000° C for 2 h in air. The synthesis of $SrTiO_3$ was checked by X-ray powder diffraction. The mixture was pressed into discs 15.0 mm in diameter and 3 mm thick at a pressure of 1000 kg cm^{-2}. The pressed discs were sintered at 1450° C for 3 h in a reducing atmosphere and furnace-cooled to room temperature.

A sintered specimen was ground to 0.3 mm thickness. Specimens for TEM observation were prepared by ion milling after removing the deformation resulting from mechanical grinding by phosphoric acid chemical polishing.

During the last decade practical stereomicroscopy has improved [13, 14], and has been used with the weak beam method for characterizing crystal defects [15, 16]. On the other hand, it is well known that the TEM weak beam method is effective for characterizing dense and complicated dislocations [17–19]. The main advantage of the weak beam method is that the dislocation image width is very much narrower (typically about 1.5 nm) than that of a conventional strong beam image (on the order of 10.0 nm) and hence higher resolution work is possible.

In electron microscopy, the parallax P is related to the tilt angle θ, total magnification of the image in the viewer M (magnification of electron microscope and stereoviewer magnification) and specimen thickness t,

$$P = 2Mt\sin(\theta/2)$$

The best stereoscopic effect is determined by the relative values of M and θ. To obtain a stereoscopic effect, the specimen was accurately tilted about the normal to the $(02\bar{2})$ plane. In this operation the Kikuchi bands were used for controlling the tilt, i.e. the $02\bar{2}$ diffraction spot was put on the $02\bar{2}$ Kikuchi band, with the transmitted beam lying on the $02\bar{2}$ Kikuchi band. In addition, the sample was positioned such that the $02\bar{2}$ normal coincided with the rotation axis of the goniometer. The $[02\bar{2}]$ reciprocal lattice vector is obtained with a tilt of $\theta = 12°$, and extensive use of the JEOL 200 cx microscope has been made to accomplish stereo-weak beam microscopy.

3. Results

The low-angle tilt boundary shown in Fig. 1 is an interface separating crystal portions A and B, and intersects a high-angle boundary at crystal C. A deformed horseshoe-shaped grain boundary is indicated by the arrow D. Following the criteria for characterizing low-angle grain boundaries, diffraction patterns were taken from crystal portions A, B and the boundary. The edge dislocation spacing was measured. The arrows E (Fig. 1) indicate the crystal lattice dislocations interacting with the grain boundary dislocations. The grain boundary edge dislocation spacing is about 25.0 nm.

The horseshoe-shaped grain boundary is shown in Fig. 2 using the weak beam method in the $\mathbf{g}(3\mathbf{g})$ condition with $|Sg| = 1.0 \times 10^{-1}$ nm^{-1}, foil normal [3 1 1] and $\mathbf{g}\cdot(\mathbf{b}\wedge\mathbf{u}) \neq 0$ for intrinsic grain boundary edge dislocations. Thus the intrinsic edge dislocations' image width is slightly larger than usual.

The enlargement of the top of the deformed low-angle tilt grain boundary is shown in Fig. 3 using various reflections. Fig. 3a is an enlargement of Fig. 2. Fig. 3b is a bright-field image taken in the $\mathbf{g} = (1\,1\,2)$ condition. Fig. 3c is a dark-field image taken in the $\mathbf{g} = (\bar{3}\,3\,0)$ condition with foil normal [1 1 2]. These figures show the distortion of a row of edge dislocations indicated by the arrows and the disappearance of the dislocations which are indicated by the arrows in Fig. 2 and arrows A and B in Fig. 3a. Therefore, the out-of-contrast dislocations' Burgers vector $\mathbf{b}_2$ is $a[00\bar{1}]$. Hence, it can be considered that the resultant dislocations would be formed at the dislocation

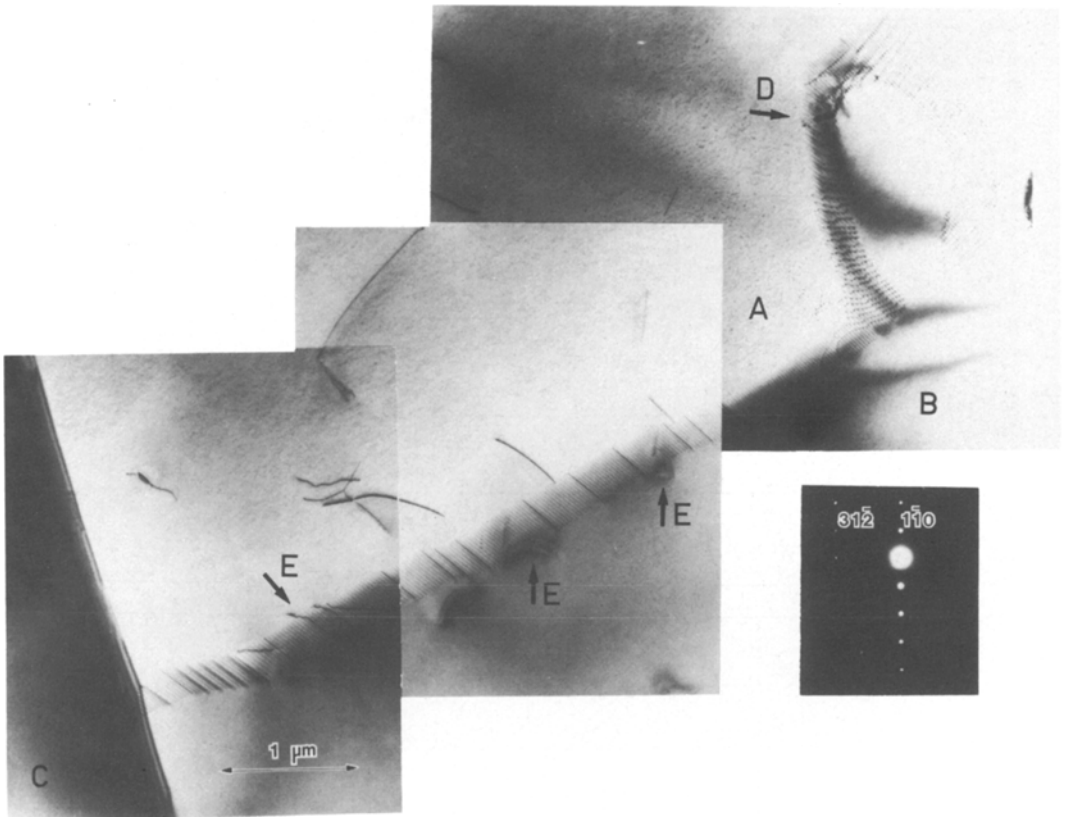

Figure 1 Bright-field image. A low-angle tilt grain boundary intersects a high-angle grain boundary. The deformed low-angle tilt boundary is indicated by the arrow D. The arrows E indicate interactions with the crystal lattice dislocations. The grain boundary edge dislocation spacing is about 25.0 nm.

networks by the following reaction:

$$\mathbf{b}_3 = \mathbf{b}_1 + \mathbf{b}_2 = a[\bar{1}00] + a[00\bar{1}] = a[\bar{1}0\bar{1}]$$

The resultant dislocations are shown by the arrows in Fig. 3a.

These two types of network shapes are shown in Figs. 3d and e. The dislocations L, M, and N have Burgers vectors $\mathbf{b}_1$, $\mathbf{b}_2$ and $\mathbf{b}_3$, respectively. L is the intrinsic grain boundary edge dislocation and N is the resultant dislocation. The Burgers vector $\mathbf{b}_2$ is parallel to the dislocation L. These configurations depend on the edge and screw components of dislocations M. In the case of Type A, the dislocations M have a large screw component; on the other hand, in Type B the dislocations M are almost pure edge.

The complex dislocation structure is indicated by the large arrow in Fig. 3a. The dislocations Q and R, which have Burgers vector $a[0\bar{1}0]$, are fixed to the boundary dislocations at the nodes q and r, respectively. Other dislocations P, O and S, which have Burgers vector $a[00\bar{1}]$, are fixed to the boundary dislocation at the nodes p, o and s, respectively.

The intrinsic edge dislocation cusps are shown in the enlargement of area A (Fig. 4). Fig. 4 is a bright-field image using the reflection $\mathbf{g} = (2\,1\,1)$. The intrinsic edge dislocations are almost perpendicular to the $2\bar{2}\bar{2}$ direction and inclined about 30° from the electron beam. The spacing of cusps for the glide direction indicated by the marker in the enlargement is about 25.0 nm. This is exactly equal to the spacing of intrinsic edge dislocations.

Stereomicroscopy has been used to characterize the three-dimensional structure of the deformed low-angle tilt grain boundary under the weak beam condition stated above with $\mathbf{g} = 02\bar{2}$ (Figs. 5a and b). It is noted that the dislocation line widths as indicated by the arrows in Figs. 5a and b increase with decreasing length of the intrinsic grain boundary edge dislocations. This suggests that the dislocations are perpendicular to the grain boundary stereoscopically. The three-dimensional structure of area A in Fig. 4 is shown schematically in Fig.

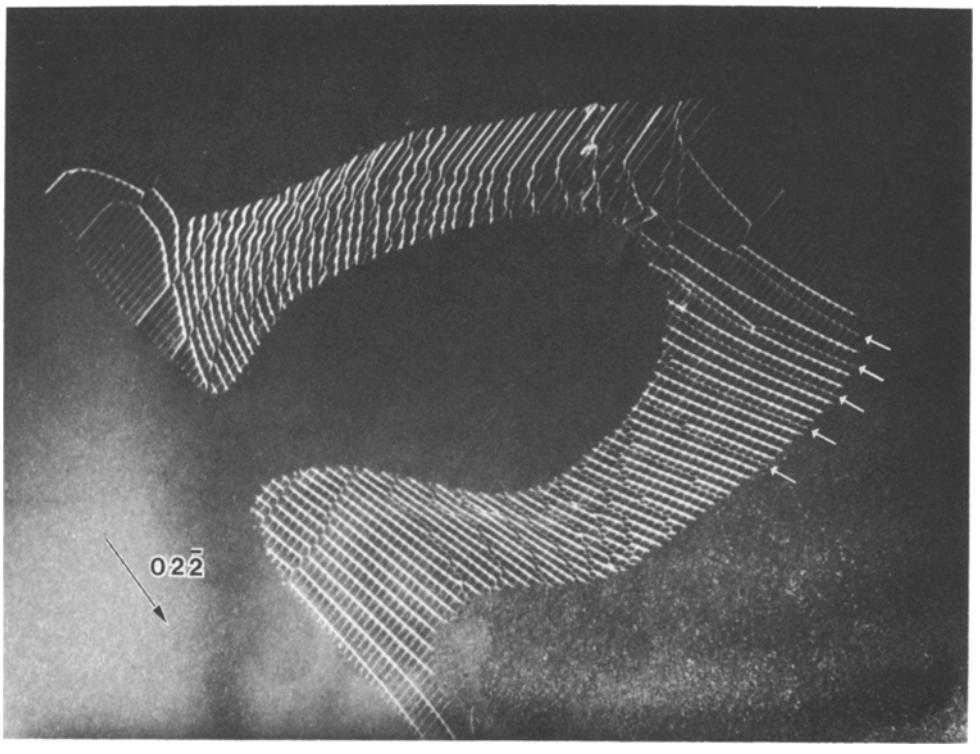

Figure 2 A weak beam dark-field micrograph of a horseshoe-shaped low-angle tilt grain boundary. Operating reflection $\mathbf{g} = 02\bar{2}$, $|Sg| = 1.0 \times 10^{-1}$ nm^{-1}, g(3g) condition.

6a, taking into account the results mentioned above. Similarly, the schematic three-dimensional structures of areas B and C are shown in Figs. 6b and c. In these figures the solid circles and the open circles represent the edge dislocation intersections with the specimen surface and the screw component intersections with the specimen surface, respectively. The solid lines and the broken lines represent the edge component and screw component, respectively. The ledge structure with the edge dislocation "partial glide" is shown in Figs. 6d and e. The term "partial glide" used here refers to the fact that only segment A′B′ of edge dislocation ABC has undergone glide. AC is an edge dislocation before deformation, A′B′C′ is the dislocation after the segment AB has glided in the direction of Burgers vector $\mathbf{b}_1$, resulting in the introduction of screw component BB′. A double array of the "partial glide" expected by a small range strain field is shown in Fig. 6e.

From these pictures, a schematic three-dimensional structure of the horseshoe-shaped low-angle tilt grain boundary was constructed (Fig. 7). The specimen thickness was measured by trace analysis to be 250.0 nm. The Burgers vector of the intrinsic edge dislocations $\mathbf{b}_1$ is $a[\bar{1}00]$, the misfit angle calculated from the edge dislocation spacing is about 0.95°, and the "partial glide" is mainly introduced at the sides of the horseshoe shape.

4. Discussion

Generally, grain boundary migration velocity is given as

$$V = MP$$

where M is mobility of the boundary and P is the driving force, equal to the free energy change per unit volume. Mobility M is a function of the migration mechanism which itself depends upon the grain boundary structure. As a result of a first approximation ignoring solute effects and assuming a single atomic process, M is expressed as follows using the Einstein equation [5]:

$$M = \frac{D\Omega}{KTr}$$

where D has the dimensions of diffusion coefficient, Ω is the atomic volume, and r is the jump distance.

Movement of boundaries in the absence of an

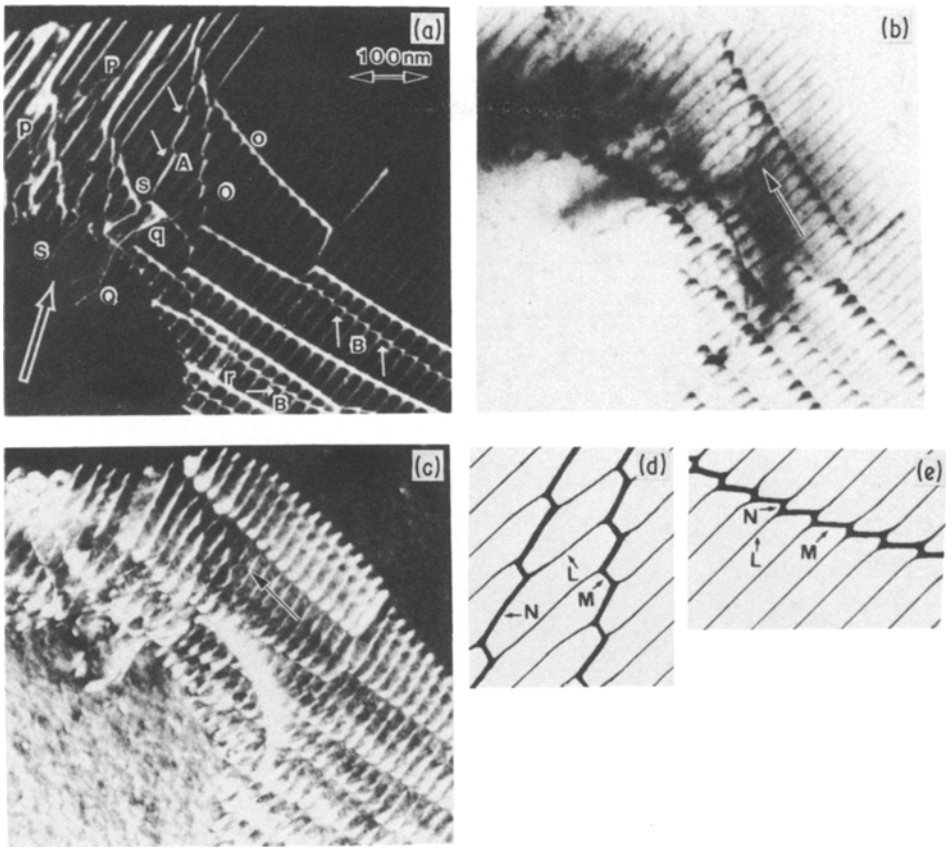

Figure 3 (a) An enlargement of the area around the top of the boundary in Fig. 2. (b) A bright-field image micrograph of the top of the boundary. Operating reflection $g = 112$. (c) A dark-field image operating reflection $g = \bar{3}30$, foil normal to [112]. (d) and (e): The dislocations L, M and N have Burgers vectors b_1, b_2 and b_3, respectively. L is the intrinsic grain boundary edge dislocation and N is the resultant dislocation. (d) shows the configuration of Type A dislocation network. The dislocation M has a large screw component. (e) shows the configuration of Type B dislocation network. The dislocation M is almost pure edge.

external stress occurs during recovery and recrystallization and requires diffusion. The most important principal feature involved is a reduction in the energy for the first stage of recovery. Drastic deformation of a low-angle tilt boundary has not been reported before and low-angle boundary migration has not been discussed extensively. In fact, coherent twins and low-angle boundaries have low mobility when compared with high-angle grain boundaries; nevertheless, it is expected that low-angle and symmetrical tilt boundaries can migrate faster by glide. The low-angle tilt grain boundary which was observed here had a very small misfit angle (about 0.95°), and thus it is expected that it would be easy for this boundary to migrate by glide with Burgers vector in the $[\bar{1}00]$ direction and $(\bar{1}00)$ plane as reported in plastic deformation studies of $SrTiO_3$ single crystals [20, 21].

In Fig. 1, arrows E indicate the grain boundary dislocation interaction with the crystal lattice dislocations, and it can be considered that the complex dislocation structure and associated networks which are shown in Figs. 2 and 3 were produced by the interaction between grain boundary dislocations and crystal lattice dislocations during the boundary glide.

In strontium titanate cubic perovskite, six oxygen atoms surround Ti ions and make octahedrons which occupy the corners of the cubic structure. These oxygen octahedrons share corners along the X, Y and Z axes. Therefore, –Ti–O–Ti–O– chains (Ti–O–Ti = 180°) are formed along the three directions. Sr ions are in the centre of the cubic structure which consists of oxygen octahedra, which is one configuration for oxygen cubic close packing. The distances between cations are as

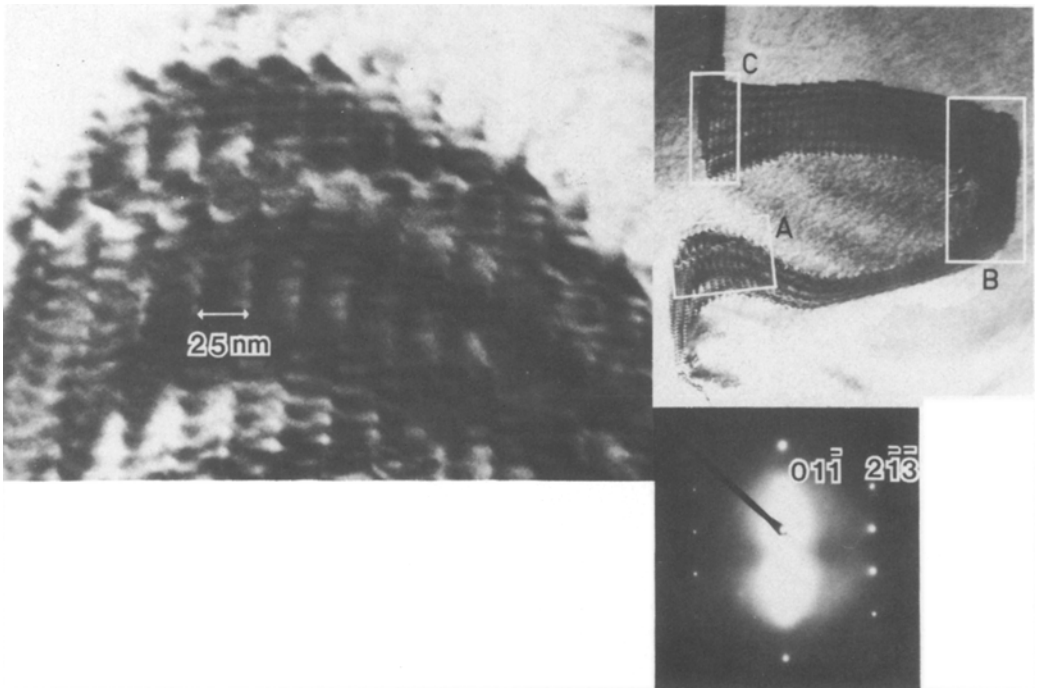

Figure 4 Bright-field image, g = 211 reflection. The intrinsic edge dislocations are almost perpendicular to the $2\bar{2}\bar{2}$ direction and inclined about 30° from the electron beam.

follows: Ti–Ti = $\sqrt{2}a$, Sr–Sr = a, and Sr–Ti = $\sqrt{(3/2)}a$. Considering the characteristics of the structure described above, the mutual interactions of cations are negligible and the main properties of strontium titanate are dependent upon –Ti–O–Ti– chains. As a result, the $(\bar{1}01)$ glide plane which would be formed by the dislocation resulting from the reaction $a[\bar{1}00] + a[00\bar{1}] = a[\bar{1}0\bar{1}]$ is not a favourable glide plane in comparison with $\{100\}$ for the perovskite structure, and the resultant dislocations are sessile. The portion of the boundary on which the dislocation network has formed by such an interaction is sessile, while the remaining portion is still glissile; therefore, the next opportunity the boundary has to glide will introduce a ledge structure between the two grains.

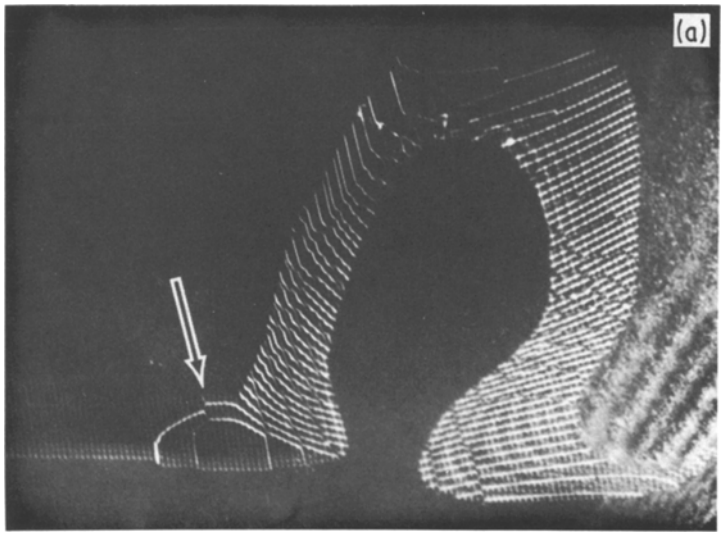

Figure 5 Weak beam g = 022 condition, the pair of stereomicrographs are tilted at 12° to each other.

Figure 5 Continued.

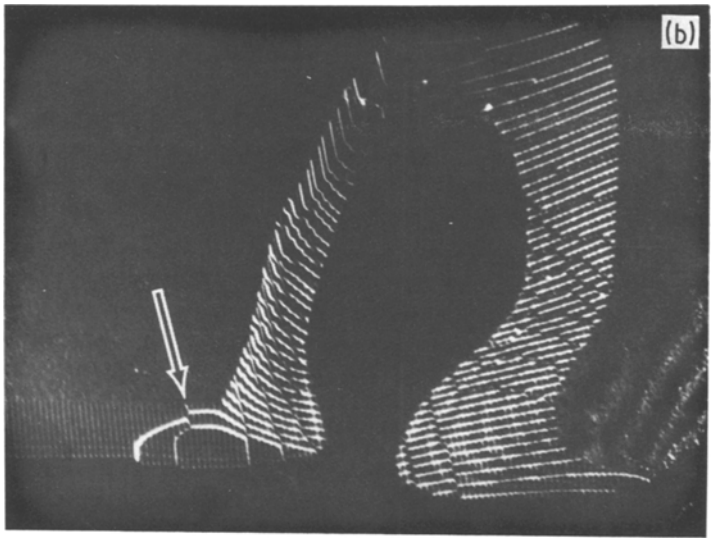

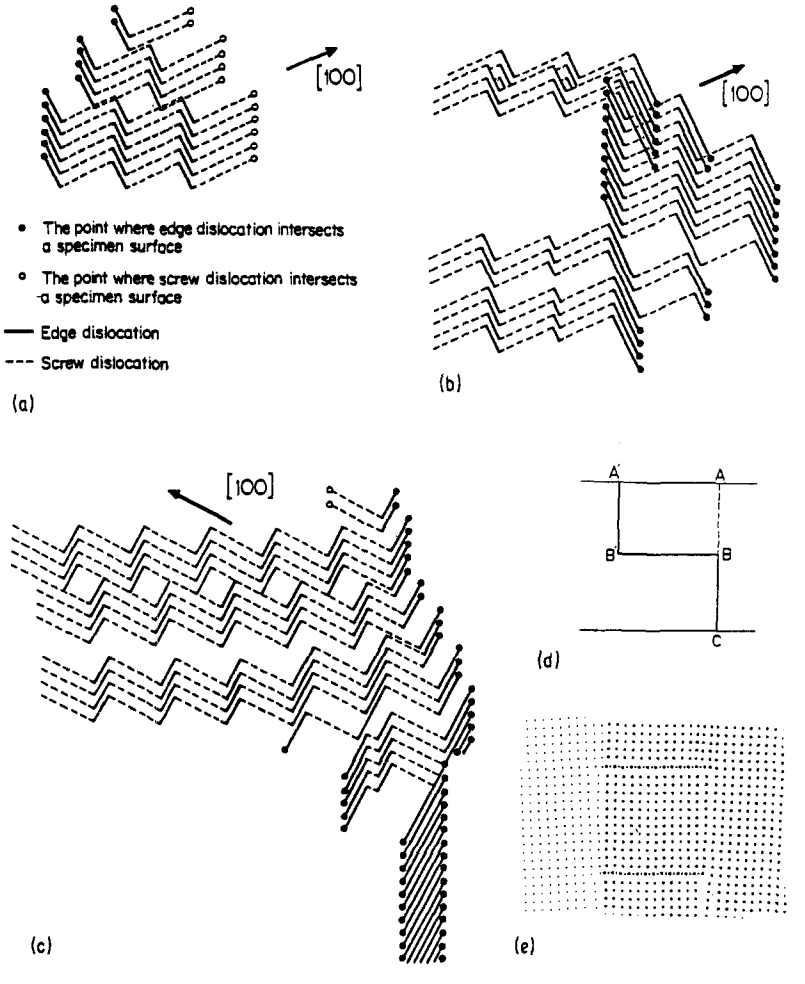

Figure 6 (a) Schematic three-dimensional structure of area A. (b) Schematic three-dimensional structure of area B. (c) Schematic three-dimensional structure of area C. The views in (a) and (c) are the reverse of one another. (d) Schematic "partial glide" structure. (e) A double array of the "partial glide" expected by a small range strain field.

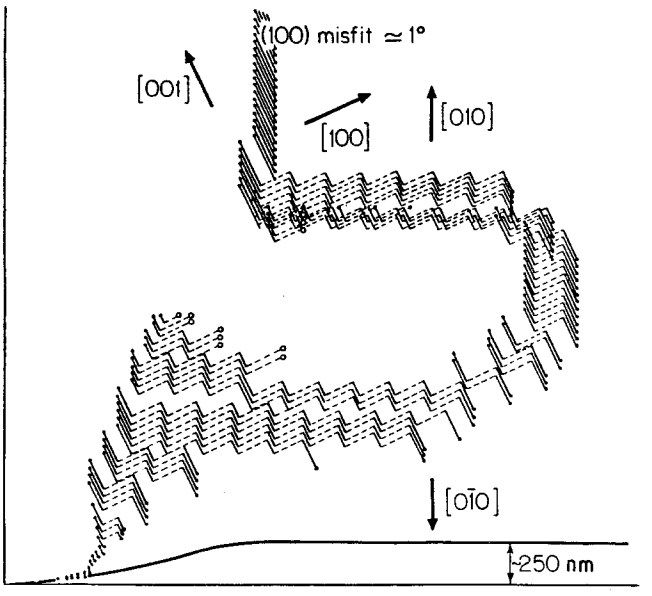

Figure 7 A schematic three-dimensional structure of a horseshoe-shaped low-angle tilt grain boundary.

Finally, the repetition of this process generates the boundary shape seen (horseshoe). The origin of this severely "deformed" low-angle tilt grain boundary is different from that of a high-angle grain boundary since there is a difference between dislocation pipe diffusion and grain boundary diffusion mechanisms. This study shows that low-angle tilt boundary glide causes interactions between grain boundary dislocations and extrinsic dislocations. It is thought, therefore, that misfit angle and formation of sessile dislocations are important in low-angle tilt grain boundary structure and migration.

5. Conclusions

1. Low-angle tilt grain boundary dislocations with Burgers vector in the ⟨100⟩ direction and {100} glide plane are observed in cubic perovskite strontium titanate.

2. The low-angle tilt grain boundary can migrate by glide. The migrating low-angle tilt grain boundary is deformed by the interactions of grain boundary dislocations with crystal lattice dislocations, which produce complex dislocation structures and dislocation networks. The resultant dislocations at the node of networks are produced by the following reaction,

$$a[\bar{1}00] + a[00\bar{1}] = a[\bar{1}0\bar{1}]$$

The resultant dislocations glide plane is $(\bar{1}01)$, which is not a favourable plane for the cubic perovskite structure. The resultant dislocations are sessile.

3. The horseshoe-shaped low-angle tilt boundary was created by the generation of obstacles (sessile dislocations in the dislocation networks) during the boundary glide.

4. The present study indicates that the weak beam method with stereomicroscopy is more useful than standard bright-field microscopy for studies of three-dimensional grain boundary structure and interactions between grain boundary dislocations and crystal lattice dislocations.

Acknowledgement

This work has been supported in part by a fellowship grant from the Taiyo Yuden Co., Ltd. and in part by the US Department of Energy under Contract No. DE-AC02-76ERO2390. Professors J. B. Vander Sande and W. D. Kingery have contributed useful discussions. Also, the author is grateful to Dr Mamoru Watanabe for useful discussions on electron diffraction.

References

1. B. CHALMERS and H. GLEITER, *Prog. Mater. Sci.* **16** (1972) 127.
2. C. J. SIMPSON, W. C. WINEGARD and K. T. AUST, "Grain Boundary Structure and Properties", edited by Chadwick and Smith (Academic Press, London, 1976) p. 201.
3. K. LUCKE, R. RIXEN and F. W. ROSENBAUM, "The Nature and Behavior of Grain Boundaries", edited by Hu (Plenum Press, New York, 1972) p. 245.
4. K. LUCKE, *Can. Met. Quart.* **13** (1974) 261.
5. D. A. SMITH, C. M. F. RAE and C. R. GROVENOR, "Grain Boundary Structure and Kinetics" (American

Society for Metals, Metal Park, Ohio, 1979) p. 337.
6. D. A. SMITH and C. M. F. RAE, *Met. Sci.* **13** (1979) 101.
7. M. F. YAN, R. M. CANNON and H. K. BOWEN, "Ceramic Microstructure 76", edited by R. M. Fulrath and J. K. Pask (1976) p. 276.
8. W. A. T. CLARK and D. A. SMITH, *J. Mater. Sci.* **14** (1979) 776.
9. R. C. POND, D. A. SMITH and P. W. J. SOUTHERDEN, *Phil. Mag. A* **37** (1978) 27.
10. M. GUILLOPE and J. P. POIRIER, *Acta Metall.* **28** (1980) 163.
11. P. G. SHEWMAN, *Trans. AIME* **230** (1964) 1134.
12. M. F. ASHBY and R. M. A. CENTAMORE, *Acta. Metall.* **16** (1968) 1081.
13. L. E. THOMAS and S. LENTZ, "Proceedings of the Conference of The Electron Microscopy Society of American" (Clators, Baton Rouge, Louisiana, 1974) p. 362.
14. W. L. BELL, *J. Appl. Phys.* **47** (1976) 1626.
15. E. L. HALL and J. B. VANDERSANDE, *Phil. Mag.* **37** (1978) 137.
16. R. M. ALLEN and J. B. VANDERSANDE, *Acta Metall.* **28** (1980) 1185.
17. D. J. H. COCKAYNE, *Z. Nature. A* **27** (1972) 452.
18. D. J. H. COCKAYNE, I. L. F. RAY and M. J. WHELAN, *Phil. Mag.* **20** (1969) 1265.
19. I. NORDLANDER and A. THOLEN, *J. Microscopy* **98** (1973) 221.
20. W. H. RHODES, *J. Amer. Ceram. Soc.* **49** (1966) 110.
21. W. H. RHODES and W. D. KINGERY, *ibid.* **49** (1966) 521.

Received 6 March
and accepted 27 March 1984